MATERIALS CHEMISTRY FRONTIERS

RESEARCH ARTICLE

View Article Online
View Journal | View Issue

Cite this: *Mater. Chem. Front.*, 2023, **7**, 1633

Efficient thermally activated delayed fluorescence emitters with regioisomeric effects for red/near-infrared organic light-emitting diodes†

Hongbo Wang,[a] Jianghui Wang,[b] Peng Zou,[b] Jingwen Xu,[b] Jinshi Li,[b] Heping Shi,*[a] Zujin Zhao*[b] and Ben Zhong Tang*[c]

Considerable efforts have been made to design efficient thermally activated delayed fluorescence (TADF) emitters for organic light-emitting diodes (OLEDs). However, the development of efficient red/near-infrared (NIR) TADF materials with emission wavelengths beyond 600 nm remains a great challenge due to serious non-radiative decay according to the energy-gap law. Herein, two novel red luminogens consisting of acenaphtho[1,2-*b*]pyrazine-8,9-dicarbonitrile (APDC) with *para*- or *ortho*-substituted cyano groups as acceptors (A) and triphenylamine (TPA) as donors (D), abbreviated as *p*-APDC-DTPA and *o*-APDC-DTPA, respectively, are designed and prepared. These luminogens are thermally stable and exhibit evident TADF characteristics. The impact of regioisomeric D–π–A–π–D structures on their TADF properties and electroluminescence (EL) behaivors is investigated and discussed, and *o*-APDC-DTPA is found to have better EL properties than *p*-APDC-DTPA. A non-doped OLED based on *o*-APDC-DTPA displays NIR light with an EL peak at 712 nm and achieves an external quantum efficiency (EQE) as high as 6.6%. The doped OLEDs employing *p*-APDC-DTPA and *o*-APDC-DTPA as emitters show red/deep red lights with EL peaks at 614–660 nm and exhibit remarkable EL performances with the highest EQEs of 10.5 and 19.0%, respectively. This work provides a reasonable design strategy and meaningful insights into the structure–property relationship for red/NIR TADF materials, which is conducive to exploring high-performance red/NIR OLEDs.

Received 13th January 2023,
Accepted 9th February 2023

DOI: 10.1039/d3qm00051f

rsc.li/frontiers-materials

Introduction

Organic light-emitting diodes (OLEDs) have aroused enormous attention and have been extensively studied owing to their potential applications in optical telecommunication, night-vision target identification, information security displays and phototherapy devices.[1] The exploration of robust and efficient luminescent materials plays a key role in the development of OLEDs, which are conducive to improving device efficiency and reducing energy consumption and manufacturing costs and are the basic premise for the large-scale commercialization of OLEDs.[2] Thermally activated delayed fluorescence (TADF) materials, as third-generation organic light-emitting materials, have been a research hotspot in the past few years,[3–9] because they are noble metal free and capable of harvesting electro-generated singlet and triplet excitons *via* a reverse intersystem crossing (RISC) process to theoretically achieve 100% internal quantum efficiency.[10–13]

In general, TADF materials are constructed into twisted molecular conformations by employing donor (D) and acceptor (A) groups to achieve sufficient separation of the highest occupied molecular orbital (HOMO) and the lowest unoccupied molecular orbital (LUMO). In this way, small energy splitting (ΔE_{ST}) between the lowest singlet excited (S_1) state and the lowest triplet excited (T_1) state can be obtained to realize the efficient RISC process.[14–21] Based on the pioneering works of Adachi's group, many efficient green and yellow TADF materials have been developed.[22–25] However, for red/near-infrared (NIR) TADF materials with photoluminescence (PL) peaks over 600 nm, they usually face the obstacle of low PL quantum yields (Φ_{PL}s), and thus poor electroluminescence (EL) performances.

[a] *School of Chemistry and Chemical Engineering, Shanxi University, Taiyuan 030006, China. E-mail: hepingshi@sxu.edu.cn*
[b] *State Key Laboratory of Luminescent Materials and Devices, Guangdong Provincial Key Laboratory of Luminescence from Molecular Aggregates, South China University of Technology, Guangzhou 510640, China. E-mail: mszjzhao@scut.edu.cn*
[c] *School of Science and Engineering, Shenzhen Institute of Aggregate Science and Technology, The Chinese University of Hong Kong, Shenzhen, Guangdong 518172, China. E-mail: tangbenz@cuhk.edu.cn*

† Electronic supplementary information (ESI) available: Materials and instruments, photophysical data, PL spectra and transient PL decay curves in the THF/water mixture, temperature-dependent transient PL decay curves, fluorescence and phosphorescence spectra at 77 K and EL data. See DOI: https://doi.org/10.1039/d3qm00051f

On one hand, the subtle overlap between the HOMO and the LUMO usually brings about a small oscillator strength and a low radiation decay rate (k_r), leading to low emission efficiency.[26–29] On the other hand, the Φ_{PL}s of red/NIR TADF materials tend to decrease dramatically as the emission wavelength increases because of the energy gap law.[30–36] Therefore, fulfilling the requirements of small ΔE_{ST} and high Φ_{PL} simultaneously is a challenge for red/NIR TADF emitters.[37–41]

There are already several strategies to develop efficient red/NIR TADF materials for application in OLEDs. For example, by delicately regulating the torsional angle of the D–A structure, small ΔE_{ST} and high k_r can be achieved simultaneously.[42,43] Incorporating rigid and planar aromatic functional groups into molecules to suppress the nonradiative decay can not only improve Φ_{PL} but also increase the PL wavelength for red/NIR TADF materials.[44,45] In addition, introducing D or A groups with large planar structures on the transition dipole moment plane of the molecule is also beneficial to improve EL efficiencies by promoting the horizontal dipole orientation and increasing the light outcoupling efficiency.[46,47] Although some red/NIR TADF emitters have been reported so far,[48–51] there is still large room for emission wavelength expansion and efficiency improvement.

According to the considerations above, in this work, two efficient red TADF molecules, 3,4-bis(4-(diphenylamino)phenyl) acenaphtho[1,2-*b*]quinoxaline-8,11-dicarbonitrile (*p*-APDC-DTPA) and 3,4-bis(4-(diphenylamino)phenyl)acenaphtho[1,2-*b*]quinoxaline-9,10-dicarbonitrile (*o*-APDC-DTPA), are designed and synthesized, which contain triphenylamine (TPA) donors and acenaphtho[1,2-*b*]pyrazine-8,9-dicarbonitrile (APDC) acceptors *para*- and *ortho*-substituted with cyano groups. Both wedge-shaped D–π–A–π–D molecules exhibit prominent TADF properties with deep-red emissions at 667 and 671 nm in pure films and relatively high Φ_{PL}s of 42% and 70% in 10 wt% doped films for *p*-APDC-DTPA and *o*-APDC-DTPA, respectively. The nondoped OLED based on *o*-APDC-DTPA exhibits NIR emission peaking at 712 nm and a maximum external quantum efficiency (EQE) of 6.6%, and the doped OLEDs based on *p*-APDC-DTPA and *o*-APDC-DTPA exhibit red lights with maximum EQEs of 10.5% and 19.0%, respectively. The EL performance of *o*-APDC-DTPA is better than that of *p*-APDC-DTPA and is comparable to those of advanced red/NIR TADF materials in the literature. These results could be used for the exploration of efficient red/NIR-TADF materials for the application in OLEDs.

Results and discussion

Synthesis and characterization

The molecular structures and synthetic routes of the target molecules *p*-APDC-DTPA and *o*-APDC-DTPA are depicted in Scheme 1. Briefly, the key intermediate **2** was synthesized by a Suzuki coupling reaction of 5,6-dibromoacenaphthylene-1,2-dione and (4-(diphenylamino)phenyl)boronic acid. Then, the target molecules were prepared by the cyclization reaction of the diketone intermediate with 2,3-diaminoterephthalonitrile and 4,5-diaminoterephthalonitrile, respectively. The molecular structures were well characterized by NMR and high-resolution mass spectra with satisfactory results (Fig. S1, ESI†).

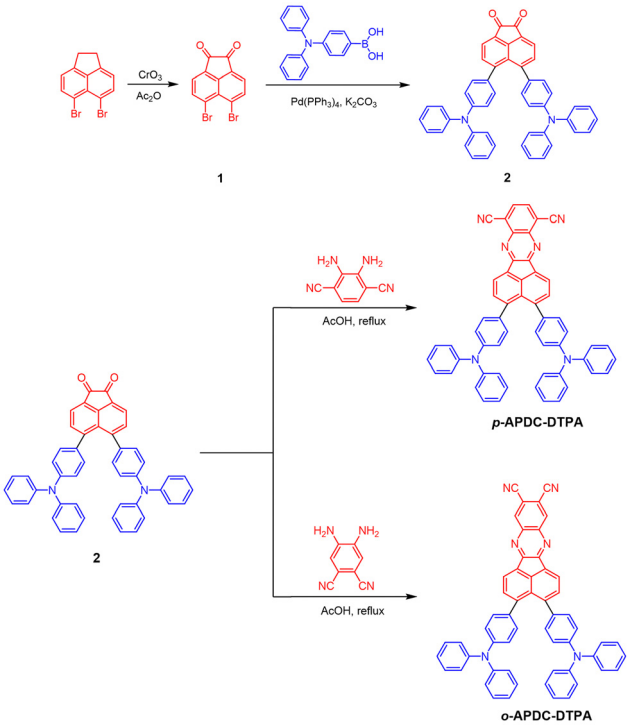

Scheme 1 Synthetic routes and chemical structures of *p*-APDC-DTPA and *o*-APDC-DTPA.

Thermal and electrochemical properties

The thermal stabilities of *p*-APDC-DTPA and *o*-APDC-DTPA were examined by thermal gravimetric analysis (TGA) and differential scanning calorimetry (DSC) to ensure their further applications in vacuum-deposited OLEDs. The results show that they have good thermal stabilities (Fig. 1A), with high decomposition temperatures (T_d, corresponding to 5% weight loss) of 476 and 481 °C for *p*-APDC-DTPA and *o*-APDC-DTPA, respectively. No clear glass-transition temperatures (T_g) were detected below 250 °C, suggesting the good morphological stability of their

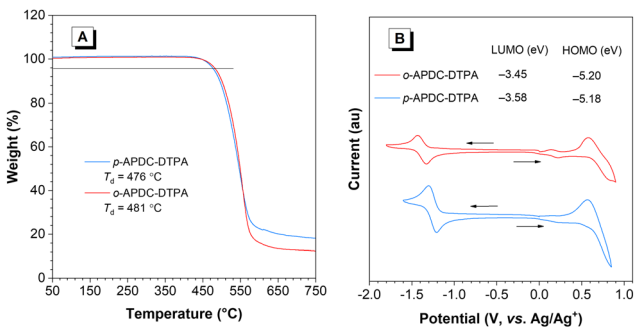

Fig. 1 (A) TGA curves of *p*-APDC-DTPA and *o*-APDC-DTPA, recorded under nitrogen at a heating rate of 10 °C min^{-1}. (B) Cyclic voltammograms of *p*-APDC-DTPA and *o*-APDC-DTPA.

amorphous films (Fig. S2, ESI†). Their electrochemical properties were investigated by cyclic voltammetry (Fig. 1B). Both molecules underwent reversible oxidation and reduction processes, indicative of their good electrochemical stability. The HOMO energy levels of *p*-APDC-DTPA and *o*-APDC-DTPA were calculated to be −5.18 and −5.20 eV, respectively, from the onsets of the oxidation curves, and the LUMO energy levels were calculated to be −3.58 and −3.45 eV, respectively, from the onsets of reduction curves.

Photophysical properties

p-APDC-DTPA and *o*-APDC-DTPA show similar absorption spectral profiles with strong absorption bands at 335 and 337 nm in toluene, respectively, which are attributed to π–π* transitions. In addition, there are broad weak absorption bands in the ranges from 442 to 451 nm, associated with the intramolecular charge transfer (ICT) states between CN–substituted APDC acceptors and TPA donors (Fig. 2A). In toluene solution, *p*-APDC-DTPA and *o*-APDC-DTPA emit orange light with emission peaks at 583 and 570 nm (Fig. 2B) and Φ_{PL}s of 48% and 62%, respectively. In order to observe their PL properties under different aggregation states, the PL spectra of these molecules in THF/H_2O mixtures with different water fractions (f_w) are measured. As shown in Fig. 2D and Fig. S3 (ESI†), the PL intensities of *p*-APDC-DTPA and *o*-APDC-DTPA become weak when f_w increases from 0 to 50 vol%, mainly due to the vigorous intramolecular motion and increased ICT effect. When f_w exceeds 50 vol%, the PL intensity is increased greatly due to the restriction of intramolecular motions in the aggregated state. It is also noticed that by adding large amounts of water to THF solution, the PL peaks are red-shifted, which is attributed to the increased polarity of the mixture and thus enhanced the ICT effect.

The neat films of *p*-APDC-DTPA and *o*-APDC-DTPA fabricated by vacuum evaporation show NIR PL peaks at 667 and 671 nm with Φ_{PL}s of 7% and 18%, respectively. The low Φ_{PL}s are mainly due to severe emission quenching by strong intermolecular π–π interactions among planar molecular structures. The doped films of *p*-APDC-DTPA and *o*-APDC-DTPA are fabricated using 2,2′,2″-(1,3,5-benzinetriyl)-tris(1-phenyl-1-*H*-benzimidazole) (TPBi) as the host at a concentration of 10 wt%, which show blue-shifted PL peaks at 631 and 620 nm (Fig. 2C) with higher Φ_{PL}s of 42% and 70%, respectively, comparable to those in toluene solutions. The Φ_{PL}s of doped films are much higher than those of non-doped films, which can be attributed to that the intermolecular interactions are alleviated to some degree by doping in the host. The mitigation of the intermolecular interaction contributes to reducing non-radiative decay of the excited state and thus improving the fluorescence rate constant (k_F) and PL efficiency. Moreover, the low temperature fluorescence and phosphorescence spectra of the doped films are recorded at 77 K (Fig. S4, ESI†), and the values of ΔE_{ST}s are measured to be 0.15 eV for *p*-APDC-DTPA and 0.08 eV for *o*-APDC-DTPA, from the onsets of the spectra. These moderate experimental ΔE_{ST}s can realize RISC processes and contribute to high exciton utilizations in OLEDs. After a delay time of 100 μs, the PL spectra of the doped films of *p*-APDC-DTPA and *o*-APDC-DTPA can still be recorded, which are similar to the prompt PL spectra (Fig. S5, ESI†), indicating the existence of delayed fluorescence. In addition, to further clarify the TADF nature of *p*-APDC-DTPA and *o*-APDC-DTPA in the solid state, temperature-

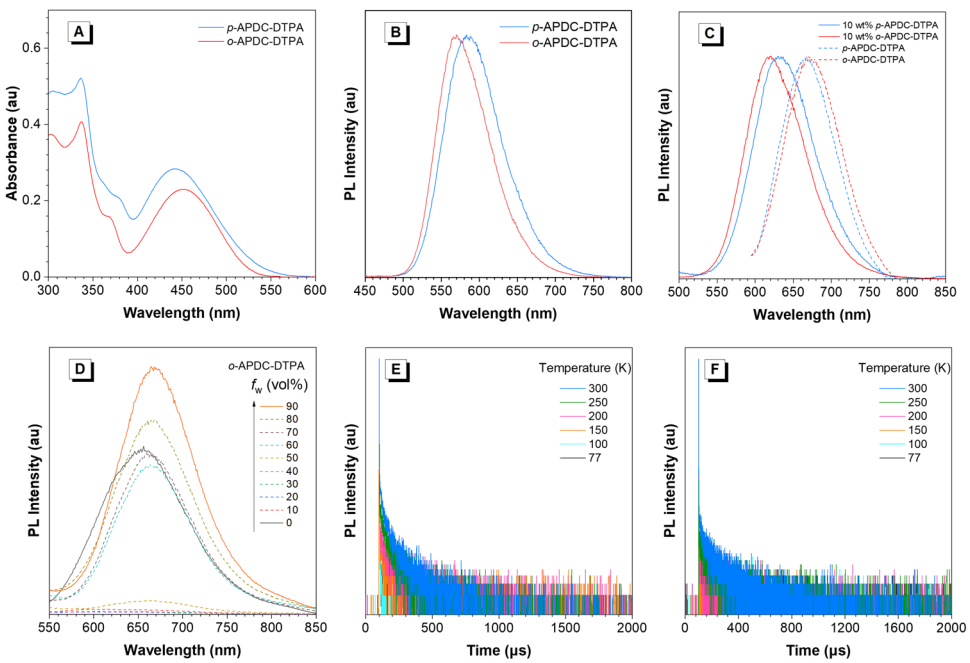

Fig. 2 (A) Absorption in toluene solution (10^{-5} M). PL spectra (B) in toluene solution (10^{-5} M) and (C) in the neat film and the doped film. (D) PL spectra of *o*-APDC-DTPA in THF/water mixtures with different water fractions (10^{-5}M). Temperature-dependent transient PL decay spectra of (E) *p*-APDC-DTPA and (F) *o*-APDC-DTPA doped films.

Table 1 Photophysical properties, energy levels, and thermal stabilities of the new molecules

Molecule	λ_{abs}[a] (nm)	λ_{em}[b] (nm) Tol/NF/DF	Φ_{PL}[c] (%) Tol/NF/DF	τ_{prompt}[d] (ns)	$\tau_{delayed}$[d] (μs)	$S_1/T_1/\Delta E_{ST}$[e] (eV)	T_d (°C)	k_F ($\times 10^7$ s^{-1})	k_{RISC} ($\times 10^4$ s^{-1})	HOMO/LUMO[f] (eV)
p-APDC-DTPA	442	583/667/631	48/7/42	2.30	69.16	2.15/2.00/0.15	476	6.9	3.7	−5.18/−3.58
o-APDC-DTPA	451	570/671/620	62/18/70	3.01	69.50	2.24/2.16/0.08	481	8.3	4.0	−5.20/−3.45

[a] Absorption maximum in toluene (Tol) solution (10^{-5} M) at room temperature. [b] Emission peak in Tol solution, neat film (NF) and doped film (DF) in TPBi (10 wt%) at room temperature. [c] Absolute PL quantum yield determined using a calibrated integrating sphere under nitrogen at room temperature. [d] The transient PL decay data of doped films in TPBi (10 wt%) at 300 K under nitrogen were fitted by a multiple-exponential function, and the prompt fluorescence lifetime (τ_{prompt}) and delayed fluorescence lifetime ($\tau_{delayed}$) were calculated by $\tau = \sum A_i\tau_i^2 / \sum A_i\tau_i$, where A_i is the pre-exponential for lifetime τ_i. [e] Estimated from the fluorescence and phosphorescence spectra of the doped film in TPBi (10 wt%) at 77 K under nitrogen. k_F = fluorescence decay rate; k_{RISC} = rate constant of reverse intersystem crossing. [f] Calculated from electrochemical data.

dependent transient PL decay spectra are measured (Fig. 2E and F). As the temperature increases from 77 to 300 K, both molecules exhibit more obvious delayed fluorescence due to the facilitation of the RISC process at high temperatures. The transient PL decay spectra of the doped films measured at 300 K reveal eminent double-exponential decay with prompt and delayed components (Table 1 and Fig. S6, ESI†). The delayed fluorescence lifetimes are fitted to be 69.16 and 69.50 μs with RISC rate constants (k_{RISC}s) of 3.7×10^4 s^{-1} and 4.0×10^4 s^{-1} for *p*-APDC-DTPA and *o*-APDC-DTPA, respectively. Apparently, *o*-APDC-DTPA has a higher Φ_{PL} and a larger k_{RISC} in the doped film than *p*-APDC-DTPA.

Theoretical calculations

To gain insights into the electronic structures of *p*-APDC-DTPA and *o*-APDC-DTPA, density functional theory (DFT) at the B3LYP/6-31G(d,p) level and time-dependent DFT (TDDFT) calculations at the M062X/6-311G(d,p) level were performed. As shown in Fig. 3, the optimized geometries of *p*-APDC-DTPA and *o*-APDC-DTPA possess dihedral angles of 51.2° and 51.5° between the APDC moiety and the phenyl bridge, respectively. Generally speaking, the HOMO and LUMO distributions of the typical TADF molecules with almost 90° dihedral angles between the donor and the acceptor are almost completely separated, which can lead to a small oscillator strength (f_s). *p*-APDC-DTPA and *o*-APDC-DTPA have relatively small dihedral angles (about 50°), which are beneficial to achieve a moderate overlap between the HOMO and the LUMO and thus increase f_s. As depicted in Fig. 3, p-APDC-DTPA and *o*-APDC-DTPA show similar HOMO distributions occupying the entire TPA donors.[52] However, the distributions of LUMOs are slightly distinguishing due to the different substitution sites of the cyano groups. For *p*-APDC-DTPA, the LUMO mainly dominates on the APDC acceptor, while for *o*-APDC-DTPA, the LUMO is more delocalized than that of *p*-APDC-DTPA, which is distributed on the whole APDC acceptor and its adjacent phenyl bridge. It follows that *o*-APDC-DTPA has a larger orbital overlap than *p*-APDC-DTPA, and f_s between the S_1 and ground (S_0) states tends to increase with larger orbital overlaps. Therefore, the *f* value of *o*-APDC-DTPA is about 0.0414, higher than that of *p*-APDC-DTPA (0.0322). Also, the larger *f* has a positive effect on k_F and Φ_{PL}. By comparing the LUMO energy levels of the two molecules, *o*-APDC-DTPA has a higher LUMO level of −2.65 eV than that of *p*-APDC-DTPA (−3.08 eV). The HOMO levels are basically the same, which are −5.17 and −5.20 eV for *p*-APDC-DTPA and *o*-APDC-DTPA, respectively. The large HOMO–LUMO gap and the relatively small distortion of the APDC-based molecules result in large ΔE_{ST}s of 0.56 and 0.58 eV for *p*-APDC-DTPA and *o*-APDC-DTPA, respectively.

Furthermore, the natural transition orbital (NTO) analyses of the excited states were performed and the corresponding transition characteristics are shown in Fig S7 and S8 (ESI†). For the S_1 states, *p*-APDC-DTPA and *o*-APDC-DTPA exhibit obvious charge-transfer (CT) characteristics, where the lowest unoccupied NTOs (LUNTOs) concentrate on the APDC acceptor, while the highest unoccupied NTOs (HONTOs) locate on TPA donors. But, for the T_1 states, both LUNTOs and HONTOs are primarily distributed on the APDC acceptor, indicative of the LE dominated characteristics. On the basis of the El-Sayed rule of the intersystem crossing (ISC) process, when the natures of S_1 and T_1 are different, the spin–orbital coupling (SOC) between S_1 and T_1 can be efficient rather than forbidden.[53,54] As expected, the SOC value between S_1 and T_1 states of *o*-APDC-DTPA is 0.372 cm^{-1}, much larger than that of *p*-APDC-DTPA (0.052 cm^{-1}). In contrast, the NTO distributions of T_2 and T_3 are the CT characteristic. In general, the up-conversion of ^{3}CT to ^{1}CT is difficult. These results disclose that the cyano groups *ortho*-substituted on the APDC acceptor have an obvious positive effect to strengthen the SOC interaction. And the promoted RISC is conducive to suppressing the nonradiative transition of the triplet excited state, thereby improving PL efficiency.

Electroluminescence

Based on the premise that these molecules have excellent photophysical properties, their applications in OLEDs as emitting layers are further investigated. The non-doped OLEDs with a configuration of ITO/HATCN (5 nm)/NPB (30 nm)/mCP (5 nm)/EML (20 nm)/TPBi (50 nm)/LiF (1 nm)/Al are fabricated, where the neat films of *p*-APDC-DTPA and *o*-APDC-DTPA serve as emitting layers (EMLs); indium-tin oxide (ITO) is the transparent anode; 1,4,5,8,9,11-hexaazatriphenylenehexacarbonitrile (HATCN) and *N,N*-bis(1-naphthyl)-*N,N*′-diphenyl-1,1′-biphenyl-4,4′-diamine (NPB) act as the hole-injecting and hole-transporting layers, respectively; 1,3-bis(carbazol-9-yl)benzene (*m*CP) is the exciton-blocking layer; TPBi acts as the electron-transporting layer; and LiF acts as the electron-injection layer, respectively. The energy level diagram and corresponding molecular structures of these functional materials are depicted in Fig. 4A and B. Table 2 lists the

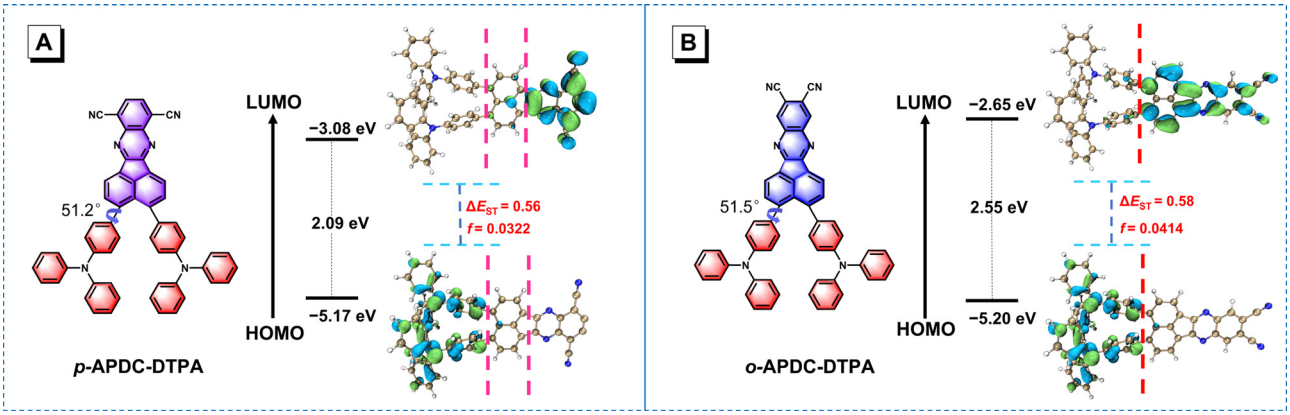

Fig. 3 Molecular structures, and calculated frontier orbital distributions and energy levels of (A) *p*-APDC-DTPA and (B) *o*-APDC-DTPA.

key data of the devices. The non-doped device based on *p*-APDC-DTPA is turned on at a voltage of 3.0 V and emits deep-red emission at 686 nm with Commission Internationale de I'clairage coordinates ($CIE_{x,y}$) of (0.657, 0.316) and an EQE of 1.2%. The non-doped device of *o*-APDC-DTPA has a lower turn-on voltage of 2.8 V, suggesting easier carrier injection and more balanced carrier transport. This device radiates NIR light with an EL peak at 712 nm ($CIE_{x,y}$ = 0.693, 0.298), which is red-shifted 28 nm compared to that of *p*-APDC-DTPA. More importantly, an impressive EQE of 6.6% is attained using this NIR device, which is comparable to those of the state-of-the-art non-doped OLEDs with NIR emissions (Table S2, ESI†).[55]

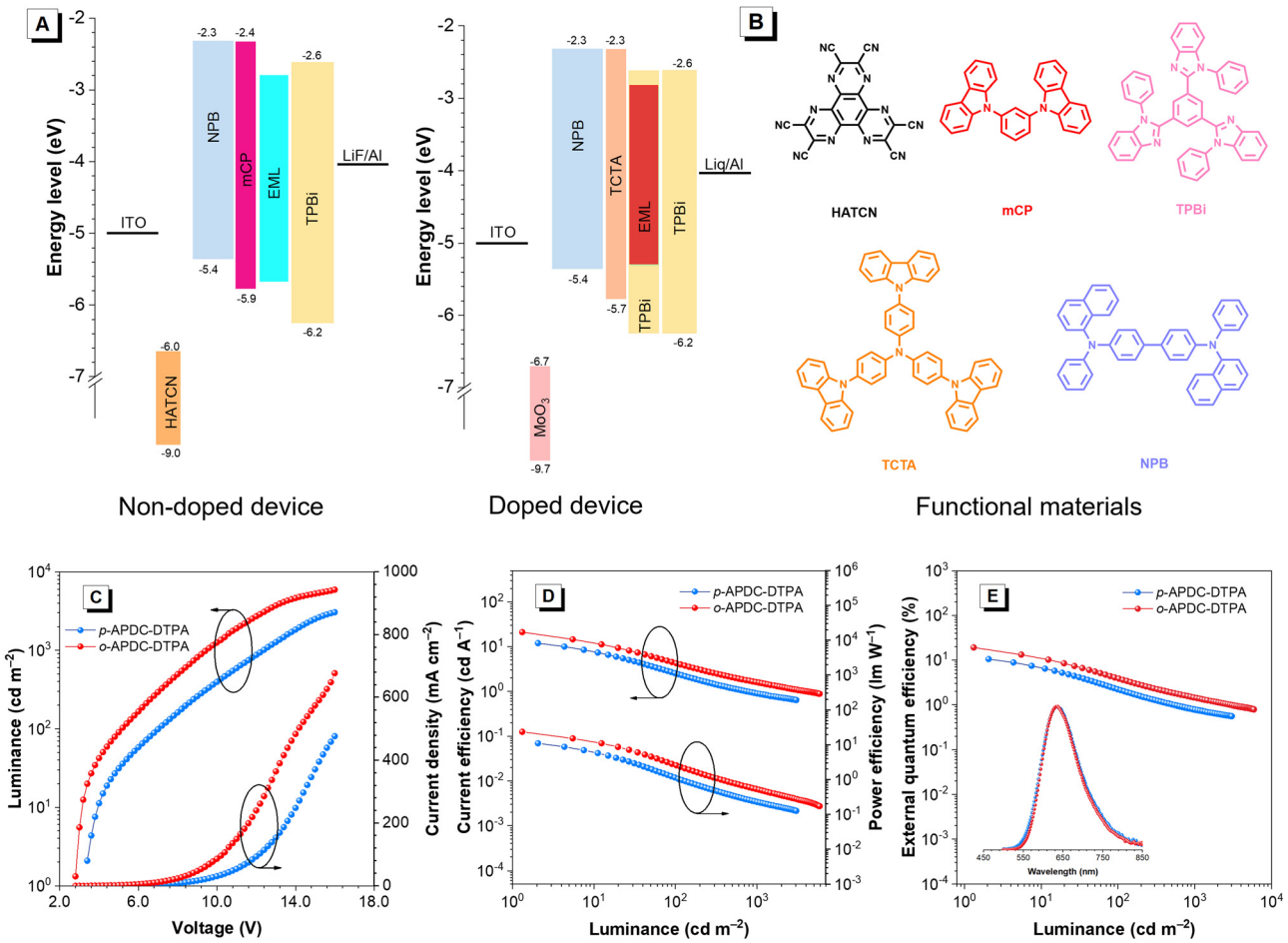

Fig. 4 (A) Device structures and energy level diagrams of non-doped and doped devices. (B) Molecular structures of the materials employed in the devices. (C) Luminance–voltage–current density, (D) current efficiency–luminance–power efficiency and (E) external quantum efficiency–luminance of the doped OLEDs with a concentration of 10 wt% in the TPBi host. Inset in plane E: EL spectra of the doped OLEDs.

Table 2 EL performances of the OLEDs based on *p*-APDC-DTPA and *o*-APDC-DTPA

Emitter	Device	V_{on}[a] (V)	L_{max} (cd m^{-2})	CE (cd A^{-1})	PE (lm W^{-1})	EQE (%)	λ_{EL} (nm)	CIE (x, y)
p-APDC-DTPA	100%	3.0	871	0.3	0.3	1.2	686	(0.657, 0.316)
	5%	3.6	5151	13.7	11.9	9.8	626	(0.597, 0.396)
	10%	3.4	3046	11.9	11.0	10.5	636	(0.618, 0.377)
	15%	2.8	2750	4.3	4.8	8.2	660	(0.668, 0.328)
o-APDC-DTPA	100%	2.8	1512	1.0	1.1	6.6	712	(0.693, 0.298)
	5%	3.6	4304	20.0	17.4	12.8	614	(0.592, 0.400)
	10%	2.8	5910	21.0	23.6	19.0	636	(0.627, 0.368)
	15%	2.8	5594	14.4	16.1	15.9	644	(0.643, 0.354)

[a] Abbreviations: V_{on} = turn-on voltage at 1 cd m^{-2}; L_{max} = maximum luminance; CE = maximum current efficiency; PE = maximum power efficiency; EQE = maximum external quantum efficiency; λ_{EL} = electroluminescence peak; CIE = Commission Internationale de l'Eclairage coordinates.

To further evaluate the potential of both molecules, doped OLEDs with varied doping concentrations (5, 10 and 15 wt%) are fabricated. The device configuration is ITO/MoO_3 (3 nm)/NPB (70 nm)/TCTA (5 nm)/x wt% emitter (x = 5, 10, and 15): TPBi (20 nm)/TPBi (70 nm)/Liq (2 nm)/Al (100 nm), in which molybdenum trioxide (MoO_3) and NPB act as the hole-injecting and hole-transporting layers, respectively; tris(4-(9*H*-carbazol-9-yl)phenyl)amine (TCTA) is the exciton-blocking layer; TPBi acts as the electron-transporting layer; and Liq acts as the electron-injection layer, respectively. Compared with the non-doped OLEDs, these doped devices show blue-shifted EL emissions and greatly enhanced EL efficiencies, which are consistent with their PL properties in neat and doped films. At a 5 wt% doping concentration, both devices display red light with EL peaks at 626 nm (CIE$_{x,y}$ = 0.597, 0.396) and 614 nm (CIE$_{x,y}$ = 0.592, 0.400), and provide maximum EQEs of 9.8 and 12.8%, respectively. The doped OLEDs at a doping concentration of 10 wt% show the best EL performance. The device based on *p*-APDC-DTPA has a turn-on voltage of 3.4 V and emits red light at 636 nm (CIE$_{x,y}$ = 0.618, 0.377) with a maximum luminance (L_{max}) of 3046 cd m^{-2}. The turn-on voltages can be reduced by optimizing device structures (Table S3, ESI†). Besides, this device exhibits a maximum current efficiency (CE), power efficiency (PE) and EQE of 11.9 cd A^{-1}, 11.0 lm W^{-1} and 10.5%, respectively. For *o*-APDC-DTPA, the doped OLED is turned on at a lower voltage of 2.8 V and exhibits red emission with a peak at 636 nm (CIE$_{x,y}$ = 0.627, 0.368) and a high L_{max} of 5910 cd m^{-2}. The maximum CE, PE, and EQE are increased to 21.0 cd A^{-1}, 23.6 lm W^{-1} and 19.0%, respectively. At a 15 wt% doping concentration, the doped OLEDs based on *p*-APDC-DTPA and *o*-APDC-DTPA display EL peaks at 660 and 644 nm, and attain high EQEs of 8.2% and 15.9%, respectively (Fig. 4 and Fig. S9–S11, ESI† and Table 2). In general, both molecules show close EL emissions but the EL efficiencies of the OLEDs based on *o*-APDC-DTPA are superior to those of *p*-APDC-DTPA-based OLEDs at various doping concentrations, which is attributed to the a relatively smaller ΔE_{ST} and a higher Φ_{PL} of *o*-APDC-DTPA.

Conclusions

In conclusion, two TADF molecules (*p*-APDC-DTPA and *o*-APDC-DTPA) composed of the TPA donor and the APDC acceptor substituted with cyano groups at the *para*- or *ortho*-positions are synthesized and characterized. They hold high thermal stability and exhibit small ΔE_{ST}s and fast RISC processes, but the Φ_{PL}s of *o*-APDC-DTPA are obviously larger than those of *p*-APDC-DTPA. Their TADF properties and EL device characteristics are also affected by the regioisomeric structures, and *o*-APDC-DTPA holds much better EL performance than *p*-APDC-DTPA. The *o*-APDC-DTPA based doped OLED exhibits a high maximum EQE of 19.0% with a red EL peak at 636 nm. Moreover, the non-doped device based on *o*-APDC-DTPA exhibits a maximum EQE of 6.6% with an EL peak at 712 nm, which is an outstanding efficiency amongst those of non-doped NIR TADF-OLEDs. This study provides valuable information for the future design of high-performance red/NIR TADF emitters based on molecular isomer engineering.

Experimental section

Synthesis and characterization

The intermediate 5,6-dibromoacenaphthylene-1,2-dione (compound **1**) was synthesized according to the literature method.[56]

5,6-Bis(4-(diphenylamino)phenyl)acenaphthylene-1,2-dione (2). A mixture of compound **1** (2.0 g, 5.88 mmol), 4-(diphenylamino) phenylboronic acid (4.2 g, 14.7 mmol), tetrakis(triphenylphosphine)palladium (0.68 g, 0.588 mmol) and potassium carbonate (2.4 g, 17.4 mmol) in the mixture of toluene, ethanol and water at a volume ratio of 8 : 1 : 1 (100 mL) was heated up to reflux and stirred for 14 h under nitrogen. After the reaction was completed, the mixture was cooled down to room temperature. The mixture was quenched with water (100 mL) and extracted with dichloromethane three times. The combined organic layers were dried with anhydrous Na_2SO_4 and concentrated by rotary evaporation. The residue solid was purified by column chromatography (silica gel) using petroleum ether/dichloromethane (1/3, v/v) as the eluent to give a 2.25 g crimson solid of compound **2** (yield: 57%). ^{1}H NMR (500 MHz, $CDCl_3$) δ 8.18 (d, J = 7.3 Hz, 2H), 7.80 (d, J = 7.3 Hz, 2H), 7.25–7.23 (m, 8H), 7.19–7.17 (m, 8H), 7.07–7.04 (m, 4H), 6.91–6.84 (m, 8H). ^{13}C NMR (125 MHz, $CDCl_3$) δ (ppm): 188.64, 148.56, 147.28, 133.70, 131.74, 130.25, 129.48, 127.88, 125.42, 123.59, 121.83, 120.60. HRMS ($C_{48}H_{32}N_2NaO_2$): m/z [M + Na$^+$] calcd 691.2335, found 691.2335.

3,4-Bis(4-(diphenylamino)phenyl)acenaphtho[1,2-*b*]quinoxaline-8,11-dicarbonitrile (*p*-APDC-DTPA). Compound **2** (600 mg, 0.9 mmol) and 2,3-diaminoterephthalonitrile (175 mg, 1.1 mmol) were added into deaerated acetic acid (40 mL) and then the suspension was heated up to reflux and stirred for 12 h under nitrogen. After cooling down to room temperature, the mixture was filtered off and washed with ethanol and then dried under vacuum. The crude product was purified by column chromatography on silica gel using hexane/dichloromethane (1/4, v/v) as the eluent and then recrystallized more than once to afford 0.36 g red solid of *p*-APDC-DTPA (yield: 50%). ^{1}H NMR (500 MHz, CD_2Cl_2) δ 8.64 (d, J = 7.3 Hz, 2H), 8.15 (s, 2H), 7.89 (d, J = 7.2 Hz, 2H), 7.29–7.20 (m, 8H), 7.19–7.09 (m, 8H), 7.08–6.96 (m, 8H), 6.92–6.79 (m, 4H). ^{13}C NMR (125 MHz, $CDCl_3$) δ 156.40, 147.42, 147.04, 146.17, 141.38, 140.11, 134.20, 132.82, 132.41, 130.78, 129.44, 128.59, 126.39, 125.32, 123.98, 123.43, 120.96, 117.42, 115.68. HRMS ($C_{56}H_{34}N_6Na$): m/z [M + Na^+] calcd 813.2727, found 813.2727.

3,4-Bis(4-(diphenylamino)phenyl)acenaphtho[1,2-*b*]quinoxaline-9,10-dicarbonitrile (*o*-APDC-DTPA). The same procedure using compound **2** (600 mg, 0.9 mmol) and 4,5-diaminoterephthalonitrile (175 mg, 1.1 mmol) was applied to afford 0.36 g red solid of *o*-APDC-DTPA (yield: 50%). ^{1}H NMR (400 MHz, CD_2Cl_2) δ 8.67 (s, 2H), 8.58 (d, J = 7.3 Hz, 2H), 7.90 (d, J = 7.2 Hz, 2H), 7.30–7.21 (m, 8H), 7.21–7.11 (m, 8H), 7.09–6.98 (m, 8H), 6.93–6.82 (m, 4H). ^{13}C NMR (125 MHz, $CDCl_3$) δ 156.96, 147.38, 147.11, 146.36, 142.43, 140.18, 136.72, 134.06, 132.53, 130.75, 129.46, 128.75, 126.53, 125.35, 123.58, 123.49, 120.90, 115.37, 112.99. HRMS ($C_{56}H_{34}N_6Na$): m/z [M + Na^+] calcd 813.2734, found 813.2734.

Conflicts of interest

There are no conflicts to declare.

Acknowledgements

This work was financially supported by the National Natural Science Foundation of China (21788102 and 21875130), the Natural Science Foundation of Guangdong Province (2022A1515010315 and 2019B030301003), the Fund of the Central Government to Guide Local Scientific and Technological Development (No YDZJSX2021A002) and the Fund of the "100 Talents Program" of Shanxi Province and the Fundamental Research Funds for the Central Universities.

Notes and references

1 C. W. Tang and S. A. VanSlyke, Organic electroluminescent diodes, *Appl. Phys. Lett.*, 1987, **51**, 913–915.
2 W. Zeng, H. Y. Lai, W. K. Lee, M. Jiao, Y. J. Shiu, C. Zhong, S. Gong, T. Zhou, G. Xie, M. Sarma, K. T. Wong, C. C. Wu and C. Yang, Achieving nearly 30% external quantum efficiency for orange-red organic light emitting diodes by employing thermally activated delayed fluorescence emitters composed of 1,8-naphthalimide-acridine hybrids, *Adv. Mater.*, 2018, **30**, 1704961.
3 Q. Zhang, J. Li, K. Shizu, S. Huang, S. Hirata, H. Miyazaki and C. Adachi, Design of efficient thermally activated delayed fluorescence materials for pure blue organic light emitting diodes, *J. Am. Chem. Soc.*, 2012, **134**, 14706–14709.
4 Y. Tao, K. Yuan, T. Chen, P. Xu, H. Li, R. Chen, C. Zheng, L. Zhang and W. Huang, Thermally activated delayed fluorescence materials towards the breakthrough of organoelectronics, *Adv. Mater.*, 2014, **26**, 7931–7958.
5 S. Hirata, Y. Sakai, K. Masui, H. Tanaka, S. Y. Lee, H. Nomura, N. Nakamura, M. Yasumatsu, H. Nakanotani, Q. Zhang, K. Shizu, H. Miyazaki and C. Adachi, Highly efficient blue electroluminescence based on thermally activated delayed fluorescence, *Nat. Mater.*, 2015, **14**, 330–336.
6 M. Y. Wong and E. Zysman-Colman, Purely organic thermally activated delayed fluorescence materials for organic light-emitting diodes, *Adv. Mater.*, 2017, **29**, 1605444.
7 J. Guo, Z. Zhao and B. Z. Tang, Purely organic materials with aggregation-induced delayed fluorescence for efficient nondoped OLEDs, *Adv. Opt. Mater.*, 2018, **6**, 1800264.
8 D. Zhang, X. Song, M. Cai, H. Kaji and L. Duan, Versatile indolocarbazole-isomer derivatives as highly emissive emitters and ideal hosts for thermally activated delayed fluorescent OLEDs with alleviated efficiency roll-off, *Adv. Mater.*, 2018, **30**, 1705406.
9 S. Shao and L. Wang, Through-space charge transfer polymers for solution-processed organic light-emitting diodes, *Aggregate*, 2020, **1**, 45–56.
10 J. Guo, X.-L. Li, H. Nie, W. Luo, S. Gan, S. Hu, R. Hu, A. Qin, Z. Zhao, S.-J. Su and B. Z. Tang, Achieving high-performance nondoped OLEDs with extremely small efficiency roll-off by combining aggregation-induced emission and thermally activated delayed fluorescence, *Adv. Funct. Mater.*, 2017, **27**, 1606458.
11 J. Huang, H. Nie, J. Zeng, Z. Zhuang, S. Gan, Y. Cai, J. Guo, S. J. Su, Z. Zhao and B. Z. Tang, Highly efficient nondoped OLEDs with negligible efficiency roll-off fabricated from aggregation-induced delayed fluorescence luminogens, *Angew. Chem., Int. Ed.*, 2017, **56**, 12971–12976.
12 J. Chen, X. Wu, H. Liu, N. Qiu, Z. Liu, D. Yang, D. Ma, B. Z. Tang and Z. Zhao, Towards efficient blue delayed fluorescence molecules by modulating torsion angle between electron donor and acceptor, *CCS Chem.*, 2022, DOI: 10.31635/ccschem.022.202202196.
13 R. Huang, Z. Yang, H. Chen, H. Liu, B. Z. Tang and Z. Zhao, *Chin. J. Chem.*, 2023, **41**, 527–534.
14 T. A. Lin, T. Chatterjee, W. L. Tsai, W. K. Lee, M. J. Wu, M. Jiao, K. C. Pan, C. L. Yi, C. L. Chung, K. T. Wong and C. C. Wu, Sky-blue organic light emitting diode with 37% external quantum efficiency using thermally activated delayed fluorescence from spiroacridine-triazine hybrid, *Adv. Mater.*, 2016, **28**, 6976–6983.
15 P. L. Dos Santos, J. S. Ward, D. G. Congrave, A. S. Batsanov, J. Eng, J. E. Stacey, T. J. Penfold, A. P. Monkman and M. R. Bryce, Triazatruxene: A rigid central donor unit for a D-A_3 thermally activated delayed fluorescence material exhibiting sub-microsecond reverse intersystem crossing and

unity quantum yield via multiple singlet-triplet state pairs, *Adv. Sci.*, 2018, **5**, 1700989.
16 Y. Liu, C. Li, Z. Ren, S. Yan and M. R. Bryce, All-organic thermally activated delayed fluorescence materials for organic light-emitting diodes, *Nat. Rev. Mater.*, 2018, **3**, 1–20.
17 C. C. Peng, S. Y. Yang, H. C. Li, G. H. Xie, L. S. Cui, S. N. Zou, C. Poriel, Z. Q. Jiang and L. S. Liao, Highly efficient thermally activated delayed fluorescence via an unconjugated donor–acceptor system realizing EQE of over 30%, *Adv. Mater.*, 2020, **32**, 2003885.
18 X. Tang, L. S. Cui, H. C. Li, A. J. Gillett, F. Auras, Y. K. Qu, C. Zhong, S. T. E. Jones, Z. Q. Jiang, R. H. Friend and L. S. Liao, Highly efficient luminescence from space-confined charge-transfer emitters, *Nat. Mater.*, 2020, **19**, 1332–1338.
19 Y. Zhang, D. Zhang, J. Wei, X. Hong, Y. Lu, D. Hu, G. Li, Z. Liu, Y. Chen and L. Duan, Achieving pure green electroluminescence with CIEy of 0.69 and EQE of 28.2% from an aza-fused multi-resonance emitter, *Angew. Chem., Int. Ed.*, 2020, **59**, 17499–17503.
20 S. Kothavale, W. J. Chung and J. Y. Lee, High efficiency and long lifetime orange-red thermally activated delayed fluorescent organic light emitting diodes by donor and acceptor engineering, *J. Mater. Chem. C*, 2021, **9**, 528–536.
21 J. Wei, C. Zhang, D. Zhang, Y. Zhang, Z. Liu, Z. Li, G. Yu and L. Duan, Indolo[3,2,1-jk]carbazole embedded multiple-resonance fluorophors for narrowband deep-blue electroluminescence with EQE $\approx$ 34.7% and CIEy $\approx$ 0.085, *Angew. Chem., Int. Ed.*, 2021, **60**, 12269–12273.
22 H. Uoyama, K. Goushi, K. Shizu, H. Nomura and C. Adachi, Highly efficient organic light-emitting diodes from delayed fluorescence, *Nature*, 2012, **492**, 234–238.
23 T.-L. Wu, M.-J. Huang, C.-C. Lin, P.-Y. Huang, T.-Y. Chou, R.-W. Chen-Cheng, H.-W. Lin, R.-S. Liu and C.-H. Cheng, Diboron compound-based organic light-emitting diodes with high efficiency and reduced efficiency roll-off, *Nat. Photonics*, 2018, **12**, 235–240.
24 Y. K. Chen, J. Jayakumar, C. M. Hsieh, T. L. Wu, C. C. Liao, J. Pandidurai, C. L. Ko, W. Y. Hung and C. H. Cheng, Triarylamine-pyridine-carbonitriles for organic light-emitting devices with EQE nearly 40%, *Adv. Mater.*, 2021, **33**, 2008032.
25 W. Li, M. Li, W. Li, Z. Xu, L. Gan, K. Liu, N. Zheng, C. Ning, D. Chen, Y. C. Wu and S. J. Su, Spiral donor design strategy for blue thermally activated delayed fluorescence emitters, *ACS Appl. Mater. Interfaces*, 2021, **13**, 5302–5311.
26 Q. Zhang, H. Kuwabara, W. J. Potscavage, Jr., S. Huang, Y. Hatae, T. Shibata and C. Adachi, Anthraquinone-based intramolecular charge-transfer compounds: computational molecular design, thermally activated delayed fluorescence, and highly efficient red electroluminescence, *J. Am. Chem. Soc.*, 2014, **136**, 18070–18081.
27 K. Wu, T. Zhang, L. Zhan, C. Zhong, S. Gong, Z. H. Lu and C. Yang, Tailoring optoelectronic properties of phenanthroline-based thermally activated delayed fluorescence emitters through isomer engineering, *Adv. Opt. Mater.*, 2016, **4**, 1558–1566.
28 S. Wang, Z. Cheng, X. Song, X. Yan, K. Ye, Y. Liu, G. Yang and Y. Wang, Highly efficient long-wavelength thermally activated delayed fluorescence OLEDs based on dicyanopyrazino phenanthrene derivatives, *ACS Appl. Mater. Interfaces*, 2017, **9**, 9892–9901.
29 J. H. Kim, J. H. Yun and J. Y. Lee, Recent progress of highly efficient red and near-infrared thermally activated delayed fluorescent emitters, *Adv. Opt. Mater.*, 2018, **6**, 1800255.
30 R. Englman and J. Jortner, The energy gap law for radiationless transitions in large molecules, *Mol. Phys.*, 1970, **18**, 145–164.
31 J. V. Caspar, E. M. Kober, B. P. Sullivan and T. J. Meyer, Application of the energy gap law to the decay of charge-transfer excited states, *J. Am. Chem. Soc.*, 1982, **104**, 630–632.
32 J. S. Wilson, N. Chawdhury, M. R. Al-Mandhary, M. Younus, M. S. Khan, P. R. Raithby, A. Köhler and R. H. Friend, The energy gap law for triplet states in Pt-containing conjugated polymers and monomers, *J. Am. Chem. Soc.*, 2001, **123**, 9412–9417.
33 F.-M. Xie, X.-Y. Zeng, J.-X. Zhou, Z.-D. An, W. Wang, Y.-Q. Li, X.-H. Zhang and J.-X. Tang, Intramolecular H-bond design for efficient orange–red thermally activated delayed fluorescence based on a rigid dibenzo [f, h] pyrido [2, 3-b] quinoxaline acceptor, *J. Mater. Chem. C*, 2020, **8**, 15728–15734.
34 Y. J. Yu, Y. Hu, S. Y. Yang, W. Luo, Y. Yuan, C. C. Peng, J. F. Liu, A. Khan, Z. Q. Jiang and L. S. Liao, Near-infrared electroluminescence beyond 800 nm with high efficiency and radiance from anthracene cored emitters, *Angew. Chem., Int. Ed.*, 2020, **59**, 21578–21584.
35 U. Balijapalli, R. Nagata, N. Yamada, H. Nakanotani, M. Tanaka, A. D'Aleo, V. Placide, M. Mamada, Y. Tsuchiya and C. Adachi, Highly efficient near-infrared electrofluorescence from a thermally activated delayed fluorescence molecule, *Angew. Chem., Int. Ed.*, 2021, **60**, 8477–8482.
36 A. Shang, T. Lu, H. Liu, C. Du, F. Liu, D. Jiang, J. Min, H. Zhang and P. Lu, Study of configuration differentia and highly efficient deep-red thermally activated delayed fluorescent organic light-emitting diodes based on phenanthro[4,5-fgh]quinoxaline derivatives, *J. Mater. Chem. C*, 2021, **9**, 7392–7399.
37 R. Furue, K. Matsuo, Y. Ashikari, H. Ooka, N. Amanokura and T. Yasuda, Highly efficient red-orange delayed fluorescence emitters based on strong π-accepting dibenzophenazine and dibenzoquinoxaline cores: toward a rational pure-red OLED design, *Adv. Opt. Mater.*, 2018, **6**, 1701147.
38 D. G. Congrave, B. H. Drummond, P. J. Conaghan, H. Francis, S. T. E. Jones, C. P. Grey, N. C. Greenham, D. Credgington and H. Bronstein, A simple molecular design strategy for delayed fluorescence toward 1000 nm, *J. Am. Chem. Soc.*, 2019, **141**, 18390–18394.
39 X. Gong, C.-H. Lu, W.-K. Lee, P. Li, Y.-H. Huang, Z. Chen, L. Zhan, C.-C. Wu, S. Gong and C. Yang, High-efficiency red thermally activated delayed fluorescence emitters based on benzothiophene-fused spiro-acridine donor, *Chem. Eng. J.*, 2021, **405**, 126663.

40 H. Yu, X. Song, N. Xie, J. Wang, C. Li and Y. Wang, Reversible crystal-to-crystal phase transitions with high-contrast luminescent alterations for a thermally activated delayed fluorescence emitter, *Adv. Funct. Mater.*, 2021, **31**, 2007511.

41 Y. Liu, J. Yang, Z. Mao, X. Chen, Z. Yang, X. Ge, X. Peng, J. Zhao, S. J. Su and Z. Chi, Asymmetric thermally activated delayed fluorescence emitter for highly efficient red/near-infrared organic light-emitting diodes, *ACS Appl. Mater. Interfaces*, 2022, **14**, 33606–33613.

42 Y. Yuan, Y. Hu, Y.-X. Zhang, J.-D. Lin, Y.-K. Wang, Z.-Q. Jiang, L.-S. Liao and S.-T. Lee, Over 10% EQE near-infrared electroluminescence based on a thermally activated delayed fluorescence emitter, *Adv. Funct. Mater.*, 2017, **27**, 1700986.

43 T. Yang, B. Liang, Z. Cheng, C. Li, G. Lu and Y. Wang, Construction of efficient deep-red/near-infrared emitter based on a large π-conjugated acceptor and delayed fluorescence OLEDs with external quantum efficiency of over 20%, *J. Phys. Chem. C*, 2019, **123**, 18585–18592.

44 P. Rajamalli, N. Senthilkumar, P. Y. Huang, C. C. Ren-Wu, H. W. Lin and C. H. Cheng, New molecular design concurrently providing superior pure blue, thermally activated delayed fluorescence and optical out-coupling efficiencies, *J. Am. Chem. Soc.*, 2017, **139**, 10948–10951.

45 T. D. Schmidt, T. Lampe, M. R. Daniel Sylvinson, P. I. Djurovich, M. E. Thompson and W. Brütting, Emitter orientation as a key parameter in organic light-emitting diodes, *Phys. Rev. Appl.*, 2017, **8**, 037001.

46 Z. Cai, X. Wu, H. Liu, J. Guo, D. Yang, D. Ma, Z. Zhao and B. Z. Tang, Realizing record-high electroluminescence efficiency of 31.5% for red thermally activated delayed fluorescence molecules, *Angew. Chem., Int. Ed.*, 2021, **60**, 23635–23640.

47 Y. L. Zhang, Q. Ran, Q. Wang, Y. Liu, C. Hänisch, S. Reineke, J. Fan and L. S. Liao, High-efficiency red organic light-emitting diodes with external quantum efficiency close to 30% based on a novel thermally activated delayed fluorescence emitter, *Adv. Mater.*, 2019, **31**, 1902368.

48 S. Wang, X. Yan, Z. Cheng, H. Zhang, Y. Liu and Y. Wang, Highly efficient near-infrared delayed fluorescence organic light emitting diodes using a phenanthrene-based charge-transfer compound, *Angew. Chem., Int. Ed.*, 2015, **54**, 13068–13072.

49 T. Yang, J. X. Liang, Y. Y. Cui, Z. Q. Li, X. M. Peng, S. J. Su, Y. Wang and C. L. Li, Achieving 34.3% external quantum efficiency for red thermally activated delayed fluorescence organic light-emitting diode by molecular isomer engineering, *Adv. Opt. Mater.*, 2023, **11**, 2201191.

50 J. L. He, Y. K. Tang, K. Zhang, Y. Zhao, Y. C. Lin, C. K. Hsu, C. H. Chen, T. L. Chiu, J. H. Lee, C. K. Wang, C. C. Wu and J. Fan, An extended π-backbone for highly efficient near-infrared thermally activated delayed fluorescence with enhanced horizontal molecular orientation, *Mater. Horiz.*, 2022, **9**, 772–779.

51 A. Q. Shang, T. Lu, H. Liu, C. Y. Du, F. T. Liu, D. Y. Jiang, J. R. Min, H. Q. Zhang and P. Lu, Study of configuration differentia and highly efficient deep-red thermally activated delayed fluorescent organic light-emitting diodes based on phenanthro[4,5-fgh]quinoxaline derivatives, *J. Mater. Chem. C*, 2021, **9**, 7392–7399.

52 T. Lu and F. Chen, Multiwfn: A multifunctional wavefunction analyzer, *J. Comput. Chem.*, 2012, **33**, 580–592.

53 D. Beljonne, Z. Shuai, G. Pourtois and J. Bredas, Spin-orbit coupling and intersystem crossing in conjugated polymers: a configuration interaction description, *J. Phys. Chem. A*, 2001, **105**, 3899–3907.

54 P. K. Samanta, D. Kim, V. Coropceanu and J. L. Bredas, Up-conversion intersystem crossing rates in organic emitters for thermally activated delayed fluorescence: impact of the nature of singlet vs triplet excited states, *J. Am. Chem. Soc.*, 2017, **139**, 4042–4051.

55 Y. Z. Shi, H. Wu, K. Wang, J. Yu, X. M. Ou and X. H. Zhang, Recent progress in thermally activated delayed fluorescence emitters for nondoped organic light-emitting diodes, *Chem. Sci.*, 2022, **13**, 3625–3651.

56 F. B. Mallory, C. W. Mallory, K. E. Butler, M. B. Lewis, A. Q. Xia, E. D. Luzik, L. E. Fredenburgh, M. M. Ramanjulu, Q. N. Van and M. M. Francl, Nuclear spin−spin coupling via nonbonded interactions. 8.1 the distance dependence of through-space fluorine−fluorine coupling, *J. Am. Chem. Soc.*, 2000, **122**, 4108–4116.